



OPEN ACCESS

Tom Millar, Queen's University Belfast, United Kingdom

Mirosław Schmidt, Polish Academy of Sciences, Poland Guillermo Quintana-Lacaci, Spanish National Research Council (CSIC), Spain

*CORRESPONDENCE Lucy M. Ziurys, □ Iziurys@arizona.edu

RECEIVED 01 July 2025 ACCEPTED 08 September 2025 PUBLISHED 17 October 2025

Ziurys LM (2025) The unique chemistry in the envelopes of massive stars. Front. Astron. Space Sci. 12:1657875. doi: 10.3389/fspas.2025.1657875

COPYRIGHT

© 2025 Ziurys. This is an open-access article distributed under the terms of the Creative Commons Attribution License (CC BY). The use, distribution or reproduction in other forums is permitted, provided the original author(s) and the copyright owner(s) are credited and that the original publication in this journal is cited, in accordance with accepted academic practice. No use, distribution or reproduction is permitted which does not comply with these terms.

The unique chemistry in the envelopes of massive stars

Lucy M. Ziurys*

Department of Astronomy, Department of Chemistry, University of Arizona, Tucson, AZ, United States

The envelopes of evolved massive stars (M ~9−40 M_o) on the Red Supergiant (RSG) Branch offer a unique situation to examine extreme circumstellar chemistry. Unlike their counterparts on the Asymptotic Giant Branch (AGB), these envelopes undergo energetic and highly-directional mass loss events, which distort a mostly spherical stellar wind. The envelope is subject to isolated shocks, grain destruction and dredge-up, all which generate a very complex chemical environment. Molecule formation involves thermodynamic equilibrium, localized shock heating, and varied elemental enrichment, frequently on timescales of a few hundred years. In this energized, oxygen-rich material, refractory oxides are synthesized, including AlO, PO, AlOH, TiO and VO, as well as metal halides (NaCl, AlCl, KCl, and AlF), but often with varying spatial distributions. High resolution imaging of molecular emission in the classic RSG, VY Canis Majoris (VY CMa) has given chemical and physical insight into these unique objects, but further studies are clearly needed.

astrochemistry, circumstellar envelopes, red supergiant stars, VY Canis Majoris, NML Cygnus, interstellar molecules, molecular abundances

1 Introduction

The study of circumstellar chemistry for many decades has focused on the envelopes of low and intermediate mass stars (M $\sim 1-8 \, \rm M_{\odot}$) that evolve onto the asymptotic giant branch, or AGB (Herwig, 2005). The reason for this selection is in part because AGB envelopes are carbon-rich, with C/O ~ 1.5. Because carbon has unique bonding properties, many AGB envelopes have a rich and varied chemistry, with the distinctive example of the famous star IRC+10216 (e.g., Tenenbaum et al., 2010a; b; Zhang et al., 2017). IRC+10216 is also in relatively close proximity to the solar neighborhood with a distance of roughly 130 pc, making the object more favorable for the detection of molecular species and chemical studies. Envelopes of oxygen-rich AGB stars have seldom received the attention of IRC+10216, although in the past decade there have been more focused observations on the O-rich types (e.g., Velilla Prieto et al., 2017; Quintana-Lacaci et al., 2007; Sanchez Contreras et al., 2015).

Molecular studies of AGB and stellar envelopes in general have principally been conducted using radio telescopes at millimeter and sub-mm wavelengths, with the measurement of gas-phase spectra of pure rotational transitions. Observations have been conducted with single-dish telescopes such as the Submillimeter Telescope (SMT) of the Arizona Radio Observatory (ARO) or the Institute de Radioastronomie Millimetrique (IRAM) 30-m antenna (see Tenenbaum and Ziurys, 2010; Tenenbaum et al., 2010a; Tenenbaum et al., 2010b; Quintana-Lacaci et al., 2016). Also interferometric imaging studies have been carried out using the Large Atacama Millimeter Array (ALMA) or at the Northern

Extended Millimeter Array (NOEMA); see Singh et al. (2023); Andrews et al. (2022); Wallström et al. (2024). Infrared and optical observations have also been essential in determining envelope structure and other properties, as well as examining dust, atomic lines and molecules without dipole moments, as needed for rotational lines (e.g., Humphreys et al., 2019).

Recently, circumstellar envelopes of more massive stars ($M \sim 9-40~M_{\odot}$) have gained chemical interest (e.g., Ziurys et al., 2007; Quintana-Lacaci et al., 2007; Tenenbaum et al., 2010a; Tenenbaum et al., 2010b; Teyssier et al., 2012). These objects, termed "Red Supergiants" (RSGs), are intrinsically oxygen-rich, but have far higher mass loss rates than their AGB counterparts, with very energetic, asymmetric, and isolated ejection events. This combination of factors spawns a different chemical environment from AGB shells. Although to date the envelopes of RSGs do not have quite the molecular inventory of, for example, IRC+10216 (e.g., Tenenbaum et al., 2010a; Tenenbaum et al., 2010b), they foster unusual species such as metal oxides and hydroxides. It is therefore becoming more apparent that these types of envelopes represent distinct chemical laboratories.

Because such massive stars are rare relative to low/intermediate ones, few have been studied in detail. The three major exceptions are the very massive objects VY Canis Majoris (VY CMa), NML Cygnus (NML Cyg), and IRC+10420. They have been the subjects of broad spectral line surveys conducted in the 1 mm band using the ARO SMT (215-280 GHz: Tenenbaum et al., 2010a; Tenenbaum et al., 2010b; Singh et al., 2021; Singh et al., 2022), at 3-4 mm with the IRAM 30-m telescope (Andrews et al., 2022) or 1 and 3 mm combined, also with IRAM (83-117 GHz; 199-277 GHz: Quintana-Lacaci et al., 2016). Spectra at 1 mm from the surveys of VY CMa, NML Cyg and IRC+10420 are shown in Figure 1 (210-286 GHz). Note that the data from VY CMa and NML Cyg look almost identical, in contrast to IRC+10420, which has fewer lines. Furthermore, in certain cases, high spatial resolution imaging has also been conducted using ALMA or NOEMA (e.g., Singh et al., 2023; Quintana Lacaci et al., 2023; Ravi et al., 2024; De Beck et al., 2025). In addition, a spectral line survey (ATOMIUM) has been conducted for a large sample of O-rich stars in the range ~213-270 GHz using ALMA (Wallström et al., 2024), which includes the three RSGs, AH Sco, VX Sgr and KW Sgr. In this case, both spatial and spectral information for these sources has been obtained, but images of only a few molecules in the survey have thus far been published. With Hershel/HIFI, Teyssier et al. (2012) observed four RSGs (NML Cyg, Betelgeuse, IRC+10420, and AFGL 2343) in high energy transitions of CO, OH and H₂O. There have also been additional general surveys of circumstellar envelopes that included a few RSGs, which targeted molecules such as CN, SO and SO₂ (e.g., Bachiller et al., 1997; Omont et al., 1993). Nonetheless, sufficient data has been assembled to provide some picture into the chemistry of these massive objects.

2 The evolutionary track and envelope creation in massive stars

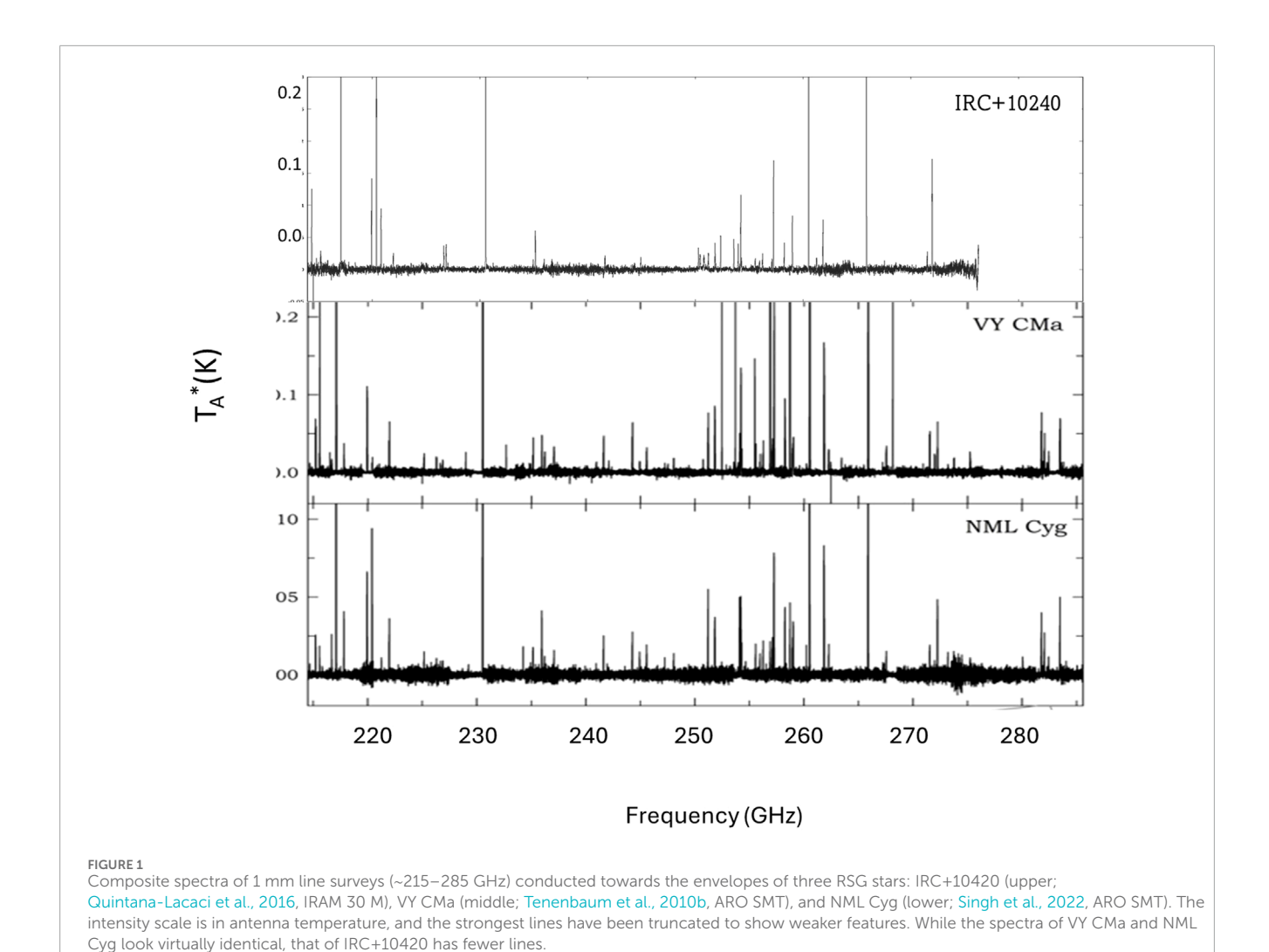
A key to understanding the chemistry in massive stars is their evolution after they leave the main sequence. Low and intermediate mass stars follow a track from the main sequence to the red giant

branch (RGB) and then onto the AGB (e.g., Milam et al., 2009). The transition to the RGB occurs with the depletion of hydrogen in the core, which burns to helium. The stellar core subsequently begins to collapse as the outer envelope expands, creating a "red giant" star (e.g., Herwig, 2005). Hydrogen-burning is sustained in a shell around a He-rich core. After sufficient collapse, the central helium ignites and starts to fuse into ¹²C. The AGB is entered when the core helium is exhausted, being converted to 12C, and the creation of a He-burning shell surrounded by an alternating Hburning one. It is during the AGB phase that mass loss increases to typical values of 10^{-8} – 10^{-5} M_{\odot} yr⁻¹, arising from dust grain formation and then acceleration by radiation pressure, long-period pulsations, and from thermal pulsing caused by interaction of the two shells (Hofner and Olofsson, 2018). This mass ejection results in a circumstellar envelope, which flows from the star and cools, forming molecules (e.g., Ziurys, 2006). With an expansion velocity of $V_{exp} \le 10-15 \text{ km s}^{-1}$, the mass loss is not overly violent and creates a roughly spherical shell. AGB stars eventually lose most of their mass and evolve into planetary nebulae, with a degenerate core that eventually transitions to a white dwarf star (Kwok, 2016).

The nature of molecule formation in circumstellar shells in part depends on the details of the nucleosynthesis. During the RGB stage, the stellar envelope encircling the core becomes highly convective, and "dredges-up" the ashes from the H-burning shell to the stellar surface. CNO cycle intermediates such as 13C and ¹⁴N reach the photosphere with large enhancements on the RGB (Milam et al., 2009). During the AGB, the main "dredge-up" product is ¹²C, created by He-fusion in the triple-alpha process (Herwig, 2005). This so-called "Third Dredge-Up" (TDU) creates "carbon stars," where C > O. It should be noted that all stars begin their evolution with C < O by about a factor of 1.5, but TDU flips the ratio in favor of carbon. Therefore, many circumstellar envelopes of AGB stars are carbon-rich, such as IRC+10216. The excess of carbon fosters an active chemistry that produces a wide variety of interstellar molecules (Tenenbaum et al., 2010a; Tenenbaum et al., 2010b; Agúndez et al., 2017; Zhang et al., 2017).

Massive RSG stars follow a somewhat different evolutionary path (Levesque, 2017). Upon depletion of hydrogen in their core, RSG progenitors will also undergo core collapse as the surrounding material expands, generating a "giant" star. An H-burning shell will ignite, followed by helium-burning in the core. Here the star enters the RSG stage. As with lower mass stars, the convective cells in the extended atmosphere will form (Lim et al., 1998) and mix products of nucleosynthesis to the surface (Ekström, 2025). However, unlike AGB stars, RSG are sufficiently massive to ignite the carbon accumulated in their cores and progress beyond C-fusion, later in their evolution creating oxygen, neon and silicon-burning shells surrounding an iron core. Their evolutionary cycle ends either as Type II-P or Type II-L supernovae, perhaps after a swing to hotter temperatures, or they may collapse quietly to black holes (Smartt, 2015). Mass ejection during these stages has a critical impact on their evolution (Smith, 2014).

The mass loss in RSGs is substantially higher than in AGB stars, with rates of 10^{-6} – $10^{-3}~M_{\odot}~yr^{-1}$, and is far more complex. In addition to a less energetic spherical wind, RSGs undergo more violent and highly directional mass loss events, occurring on timescale of a hundred years (e.g., Humphreys and Jones, 2022). These isolated ejecta are thought to arise from large convective cells in the extended



atmosphere, perhaps powered by twisted magnetic fields (Ekstrom and Georgy, 2025). They create an irregular circumstellar envelope consisting of knots, arcs and clumps extending as far as $\sim\!1000~R_{\circ}$ from the star. RSGs are also relatively cool ($T_{\rm eff}\sim3400{-}4000~K$), but are larger, somewhat warmer and more luminous than AGB stars, with R* $\sim300{-}1500~R_{\odot}$ and log L/L $_{\odot}\sim4.5{-}5.71$ (Levesque, 2017). RSGs on the higher end of the mass loss and luminosity range are termed Red Hypergiants and Yellow Hypergiants (YHGs). YHGs are thought to be post-RSG objects evolving to higher temperatures (Smith, 2014; Gordon and Humphreys, 2019), and may have somewhat detached circumstellar envelopes (Teyssier et al., 2012). VY CMa is a classic example of a Red Hypergiant star.

The complexity of RSG envelopes, as illustrated by VY CMa, is shown in Figure 2. Figure 2a (left) displays an image of emission at 230 GHz of the $J=2 \Rightarrow 1$ line of CO across the envelope of VY CMa (Singh et al., 2023). The image was created from ALMA data taken with 0.2''-1.5'' spatial resolution combined with single-dish data (30" resolution) such that there is no missing flux. CO is thought to be an excellent tracer of envelope structure (Teyssier et al., 2012; Decin et al., 2006). The envelope clearly displays a non-spherical geometry with multiple distinct structures, which are marked on the figure by letters. Many of the individual structures are seen in HST

images of dust emission from reflected starlight (Humphreys et al., 2007), as presented in Figure 2b (middle). Figure 2c shows the HST image in greyscale, with the major envelope "features" qualitatively indicated. There is almost a one-to-one correspondence between the dust and CO features except to the north-east (NE), where heavy extinction has obscured reflected starlight. Most notable in the CO and dust data are Arc 1, Arc 2, and the NW Arc. The NE structures are exclusive to CO. ALMA observations of VY CMa in SO and H_2O on a smaller spatial scale ($\sim 0.36''$) also show complexity with several inner collimated outflows disrupting a slower expanding wind (Quintana-Lacaci et al., 2023). NML Cyg has a similar overall complexity, although it has not been as thoroughly studied (see Singh et al., 2023; De Beck et al., 2025). IRC+10240, Betelgeuse and other RSGs did not appear to have such complicated envelopes (see Ziurys and Richards, 2025). This property may reflect lower mass loss rates (Betelgeuse), an older evolutionary stage (IRC+10420; Teyssier et al., 2012), or the lack of strong magnetic fields to drive the collimated flows (Quintana-Lacaci et al., 2023).

The structures observed in the images of RSG circumstellar shells are also reflected in the line profiles for stars like VY CMa and NML Cyg. In certain molecules, asymmetric profiles are observed, indicating a combination of highly-directional, red and

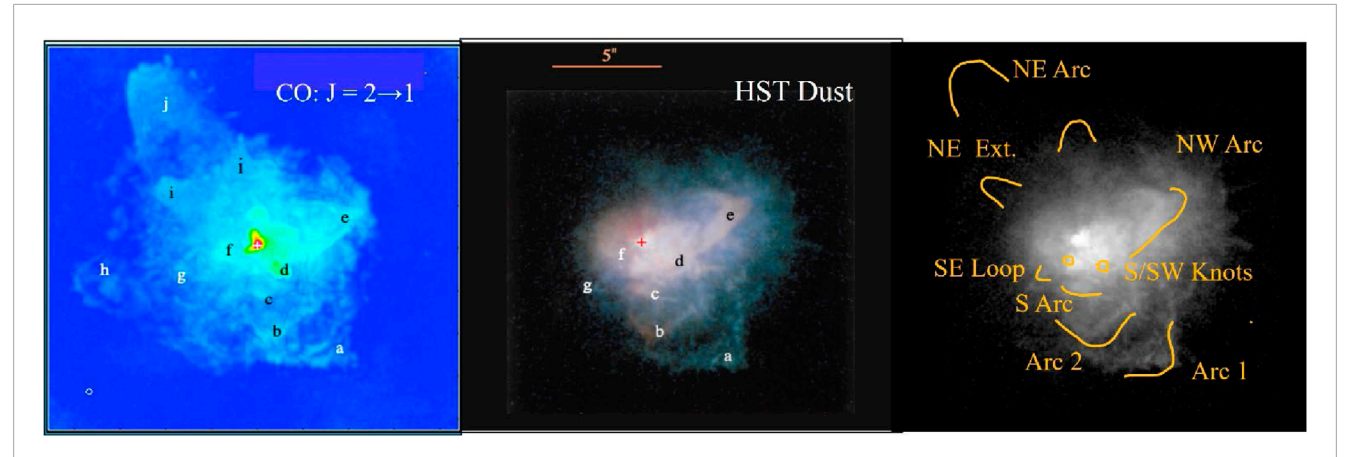


FIGURE 2 The structures in the envelope of VY CMa, as illustrated by the ALMA map of 12 CO ($J=2\rightarrow1$) (left), composite color HST dust image (middle), and black/white HST image, with major features superimposed as a cartoon (right), all displayed on the same scale (Singh et al., 2023). Star position is given by a cross (white: ALMA; red: HST). Individual features are also labeled a-j on the ALMA and color HST images; some appear in both images but others are unique to CO: a) Arc 1 b) Arc 2 c) S Arc d) SW Clump e) NW Arc f) S Knot g) SE Loop h) E Bubble i) NE Extension j) NE Arc. The major features appear in the cartoon.

blue shifted outflows relative to a spherical wind. In contrast, in AGB envelopes, the line profiles for lower opacity transitions are mostly symmetric and rectangle-like, typically flat-topped or U-shaped, depending on the coupling of the source with the telescope beam. These lines thus enable modeling using spherically-shaped shells. Figure 3 displays spectra at 235 GHz for the AGB star IRC+10216 (upper) and VY CMa (lower), plotting on the same frequency scale (Tenenbaum et al., 2010b). In the IRC+10216 data, the prominent SiC_2 feature shows the U-shape while others are flat-topped. The inset on the right shows two $\mathrm{C}_4\mathrm{H}$ features near 238 GHz with even deeper "U"s. In the VY CMa spectrum, the lines are broader and not rectangular, with the stronger SO_2 feature showing asymmetric blue and red-shifted components; the other lines are triangular in shape.

3 Molecular composition of the envelopes of massive stars

Although the envelopes of RSGs may not appear to contain the chemical inventory of C-rich AGB stars such as IRC+10216 (e.g., Tenenbaum et al., 2010a; b), this result could reflect the lack of observations and/or their relative distances to Earth. Neither VY CMa nor NML Cyg are as close as IRC+10216 (1.2 and 1.6 kpc vs. 130 pc: Ziurys and Richards, 2025). RSGs are also oxygen-rich (C/O ~ 0.5). Laboratory work is needed to detect new molecules, and a major focus of lab measurements has been oriented towards those containing carbon (see Ziurys, 2024), introducing another selection effect.

Table 1 gives the current list of molecules identified in the envelopes of massive stars. This compilation primarily reflects the composition of the envelope of VY CMa, and, in turn, that of NML Cyg, which is almost identical (Singh et al., 2022). Note that AlOH, AlCl, and AlF have yet to be identified in NML Cyg. The only species in the list that is not found in VY CMa is $\rm N_2H^+$, but further searches may prove otherwise. This molecule has thus far only been identified

in IRC+10420 (Quintana-Lacaci et al., 2016). Besides the species listed, various silicon isotopologues of SiS and SiO are found (²⁹SiS, ³⁰SiS, ²⁹SiO, ³⁰SiO), as well as ¹³CO, H¹³CN, Si³⁴S and SO¹⁸O, among other species (e.g., Singh et al., 2022; Tenenbaum et al., 2010a).

As is shown in the table, many common interstellar molecules are found in massive envelopes, starting with H2 and CO. This list includes oxygen-bearing species such as OH, SiO and H2O, typically found in the envelopes of O-rich stars (e.g., Verheyen et al., 2012; Baudry et al., 2023). Small carbon-containing compounds are also present (HCN, HNC, CN, CS, and HCO+), as originally noted by Ziurys et al. (2009). These authors suggested that these C-bearing molecules are produced by a combination of shocks, as seen in VY CMa and NML Cyg, and photochemistry. Sulfur-bearing molecules also play a dominant role as SO, SO₂, SiS, NS, H₂S (and CS). In fact, the 1 mm spectrum of VY CMa is dominated by lines of SiS, SO, and SO₂ (Tenenbaum et al., 2010a). These molecules have been detected in either C-rich or O-rich circumstellar envelopes for decades (e.g., Omont et al., 1993; Bachiller et al., 1997; Tenenbaum et al., 2010a; Tenenbaum et al., 2010b). NH3 has also been identified in RSG envelopes (Menten et al., 2010; Teyssier et al., 2012). Beyond these common molecules, circumstellar gas in massive stars also contains unusual species, with many of their first interstellar detections occurring towards VY CMa. These molecules include PO (Tenenbaum et al., 2007), AlO (Tenenbaum and Ziurys, 2009), AlOH (Tenenbaum and Ziurys, 2010), TiO, TiO₂ (Kaminski et al., 2013), and VO (Humphreys et al., 2019). In addition, PN, AlCl, AIF, NaCl and KCl have been identified in VY CMa; the sodium, potassium and aluminum halide compounds had been found in IRC+10216 prior or to their detection in VY CMa (e.g., Cernicharo and Guelin, 1987); PN was found simultaneously in VY CMa and other circumstellar shells (Milam et al., 2008), having been initially identified in molecular clouds (e.g., Ziurys, 1987).

Metal and refractory oxides thus characterize the unique chemical composition of these envelopes. Since their initial detection in VY CMa, several of these molecules have been observed in AGB shells, including AlO and PO (Decin et al., 2016; Ziurys et al.,

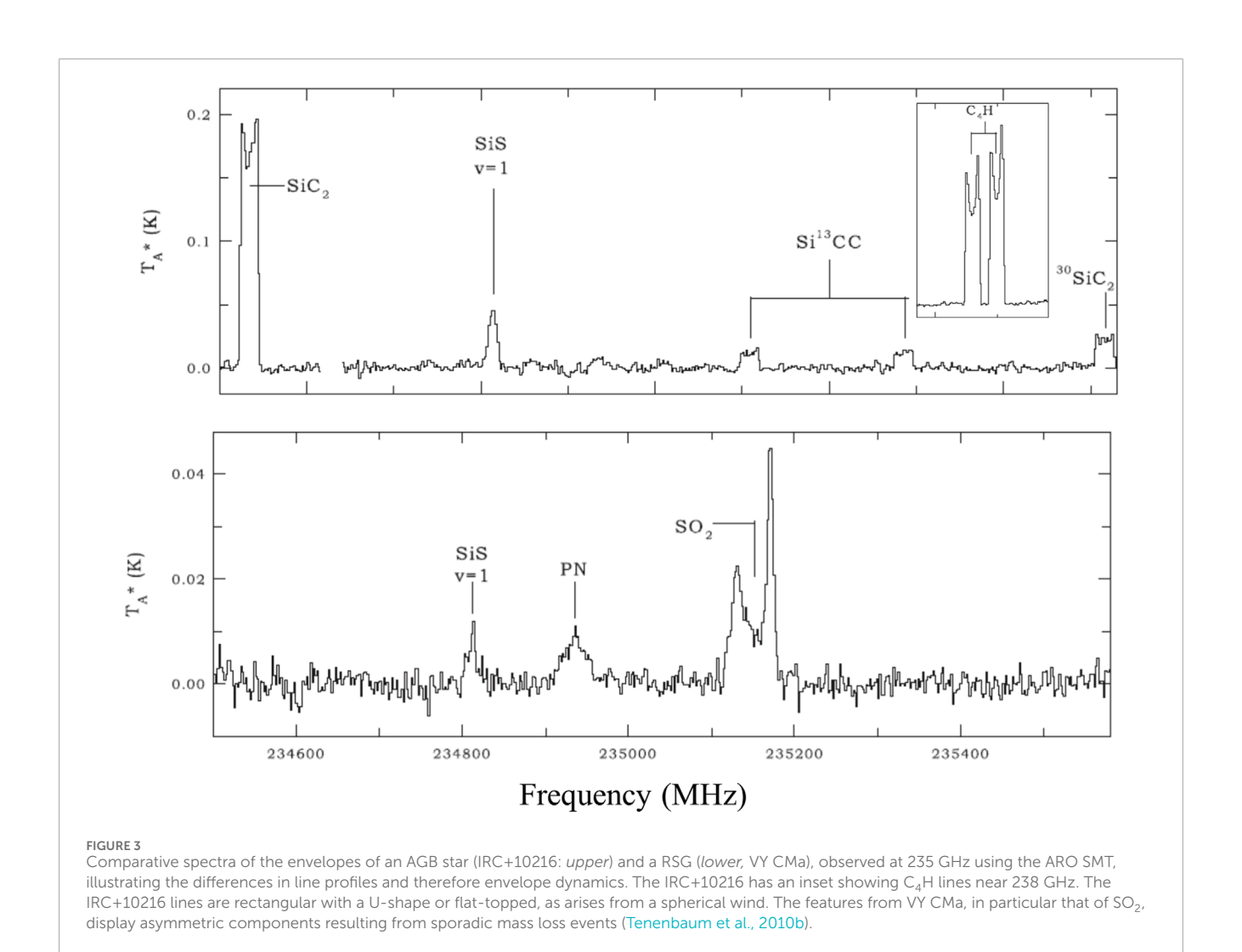


TABLE 1 Molecules detected in envelopes of massive stars.^a

H_2	HCN	SiO	PN	AlO
СО	HCO ⁺	SiS	PO	VO
CS	HNC	SO ₂	NaCl	AlOH
CN	H ₂ O	SO	KCl	TiO
NO	N ₂ H ^{+b}	NS	AlCl	TiO ₂
ОН	NH ₃	H ₂ S	AlF	

^aMillimeter-wave detections except VO (see text).

2018). However, no other O-rich AGB star has shown the chemical complexity of VY CMa to date. Furthermore, a substantial subset of the species in Table 1 have not been identified in IRC+10420, including all the metal halides and oxides, as well as PO. The only refractory molecule detected in IRC+10420 is PN.

The lack of chemical complexity in IRC+10420 is likely a result of its age and its evolution to a YHG. The star has become warmer than

VY CMa and NML Cyg. Apparently, this elevation in temperature has altered its inner envelope, which has decreased in density and therefore does not excite higher energy transitions of CO and water (Teyssier et al., 2012). The molecular envelope in IRC+10420 appears to be "hollow" and detached from the photosphere. The warmer, dense material found near ~10-20 R* that has not yet reached the terminal expansion velocity is seemingly diminished in IRC+10420. This critical region appears to foster the metal oxides and halides, as grain condensation is in the process and not yet complete (Ravi et al., 2024; Ravi et al. 2025a; Ravi et al. 2025b). Refractory molecules are still in the gas phase in considerable abundance in this inner shell region. In addition, IRC+10420 appears to have less episodic mass loss that is highly characteristic of VY CMa and NML Cyg. Such mass loss fosters chemistry-inducing shocks seen in molecules such as SO, SO₂, and H₂S (Adande et al., 2013; Quintana-Lacaci et al., 2023; Ziurys and Richards, 2025).

Representative molecular abundances found in these stars are presented in Table 2. These values are derived for VY CMa and NML Cyg and were determined typically from radiative transfer modeling of observed spectral lines; the ranges given reflect the two sources. There are currently limited radiative transfer analyses for abundances in IRC+10420, making comparison difficult. Also,

bIRC+10420 only.

as a YHG, the star has progressed beyond the RSG stage and is less chemically active. There are both spherical and asymmetric outflows in VY CMa and NML Cyg. These components have been modeled for certain molecules, and are indicated in the table (e.g., Singh et al., 2022; Adande et al., 2013). Abundances listed are summed over multiple components, if they have been modeled. The values between VY CMa and NML Cyg vary usually by no more than a factor of 5.

As the table demonstrates, aside from H₂, CO, H₂O and OH are the most abundant molecules in these types of envelopes, as might be expected in an oxygen-rich environment. They have abundances, relative to H₂, near $f \sim 10^{-4}$. The next most prevalent species is SiO, with $f \sim 10^{-5}$, followed by HCN, NH₃, SiS, and H₂S ($f \sim 10^{-6}$), and then by CS, SO, SO₂, CN and, surprisingly, PO ($f \sim 10^{-7}$). Less in abundance by another order of magnitude ($f \sim 10^{-8}$) are HNC, HCO⁺, NS, AlO, AlOH, AlCl, AlF and PN. The other metal oxides and halides (VO, TiO, NaCl) follow with $f \sim 10^{-9}$, with the least prevalent being KCl and TiO₂. The current abundance of NO is not well-determined. The values are obviously influenced in part by intrinsic photospheric, elemental abundances.

It is striking that the phosphorus compounds PO and PN are quite prevalent, given that other refractory compounds such as AlO have lower abundances, and that, cosmically, $P/H_2 = 5.2 \times 10^{-7}$ (Asplund et al., 2009). As suggested by Ravi et al. (2024), this result could reflect phosphorus production in RSG stars, or shock destruction of P-bearing grains. Also of note is the AlOH/AlO >1, suggesting the possible presence of other metal hydroxides such as TiOH and VOH. The ratio [HCN]/[HNC] of 33 indicates that both molecules reside in warmer gas (Goldsmith et al., 1986).

4 Insight into the chemistry

As discussed, the envelopes of massive stars are more complex than the typical AGB star and have many more distinct structures. A somewhat spherical, radiation-pressure driven, slow-moving wind is still present, but significantly distorted by asymmetric ejecta, as well-illustrated in Figure 1. The envelope of VY CMa in CO and in dust emission is far from spherical. Different molecules appear in various isolated regions, formed by varying chemical processes. This variation is illustrated in Figures 4–6, which show ALMA images of AlO, AlOH, AlCl, PO, PN and other molecules in the envelope of VY CMa. The images were created from combined ALMA/SMT data such that all flux is recovered (see Singh et al., 2023). Such spatial variation is also observed closer to the star, where SO and SO₂ appear to trace the spherical wind, and H₂S and NaCl the more collimated outflows (Quintana-Lacaci et al., 2023).

Near the stellar photosphere (within $\sim 50 \, \text{R}_{\bullet}$) a series of species are synthesized under conditions of Local Thermodynamic Equilibrium (LTE). The concept of LTE chemistry has been successfully used to estimate abundances in the inner envelopes of AGB evolved stars for decades (e.g., Tsuji, 1973; McCabe et al., 1979; Willacy and Cherchneff, 1998; Agúndez et al., 2017). The high densities ($n \sim 10^{10}$ – 10^{11} cm⁻³) and temperatures (T ~ 1000 –2000 K) in these regions (both in AGB and RSG stars) results in the

TABLE 2 Representative abundances in envelopes of massive stars.^a

Molecule	f (X/H ₂) ^b
СО	$1-3 \times 10^{-4}$
HCN	$1-3 \times 10^{-6c,d}$
ОН	~10 ⁻⁴
HNC	$3-9 \times 10^{-8d}$
CN	$0.5 - 2 \times 10^{-7}$
SO ₂	6-7 × 10 ^{-7 d}
SO	3 - 4 × 10 ^{-7d}
H ₂ O	$2-3 \times 10^{-4c,e}$
HCO ⁺	$3-4 \times 10^{-8}$
NH ₃	3-5×10 ^{-6f}
CS	$0.3-2 \times 10^{-7}$ d
SiO	3×10 ^{-5c}
SiS	$0.2-2 \times 10^{-6d}$
H_2S	$1-5 \times 10^{-6}$
NaCl	$3-5 \times 10^{-9}$ d
PN	$0.4-8 \times 10^{-8}$ d
PO	$0.7 - 1.4 \times 10^{-7}$
NO	~10 ⁻⁹
NS	$\sim 10^{-8} - 10^{-7} \mathrm{d}$
AlO	$0.6 - 7 \times 10^{-8}$
AlOH	9 × 10 ⁻⁸
TiO	4×10^{-9} g
TiO ₂	6×10^{-10g}
VO	~10 ⁻⁹
KCl	1.2×10^{-10}
AlCl	2 × 10 ⁻⁸
AlF	~10 ⁻⁸

^aBased on VY CMa, NML Cyg.

^bFrom Ziurys et al., 2009; Singh et al., 2022; Ravi et al., 2024, 2025a,b;

Ziurys et al., 2007, 2018.

cRover et al., 2010.

 $^{^{}m d}$ Includes central component and asymmetric outflows (SW, clump; SW, fan, $\it{etc.}$, for VY CMa: see text).

^eNeufeld et al., 2021.

^fMenten et al., 2010; Teyssier et al., 2012.

gKaminski et al., 2013.

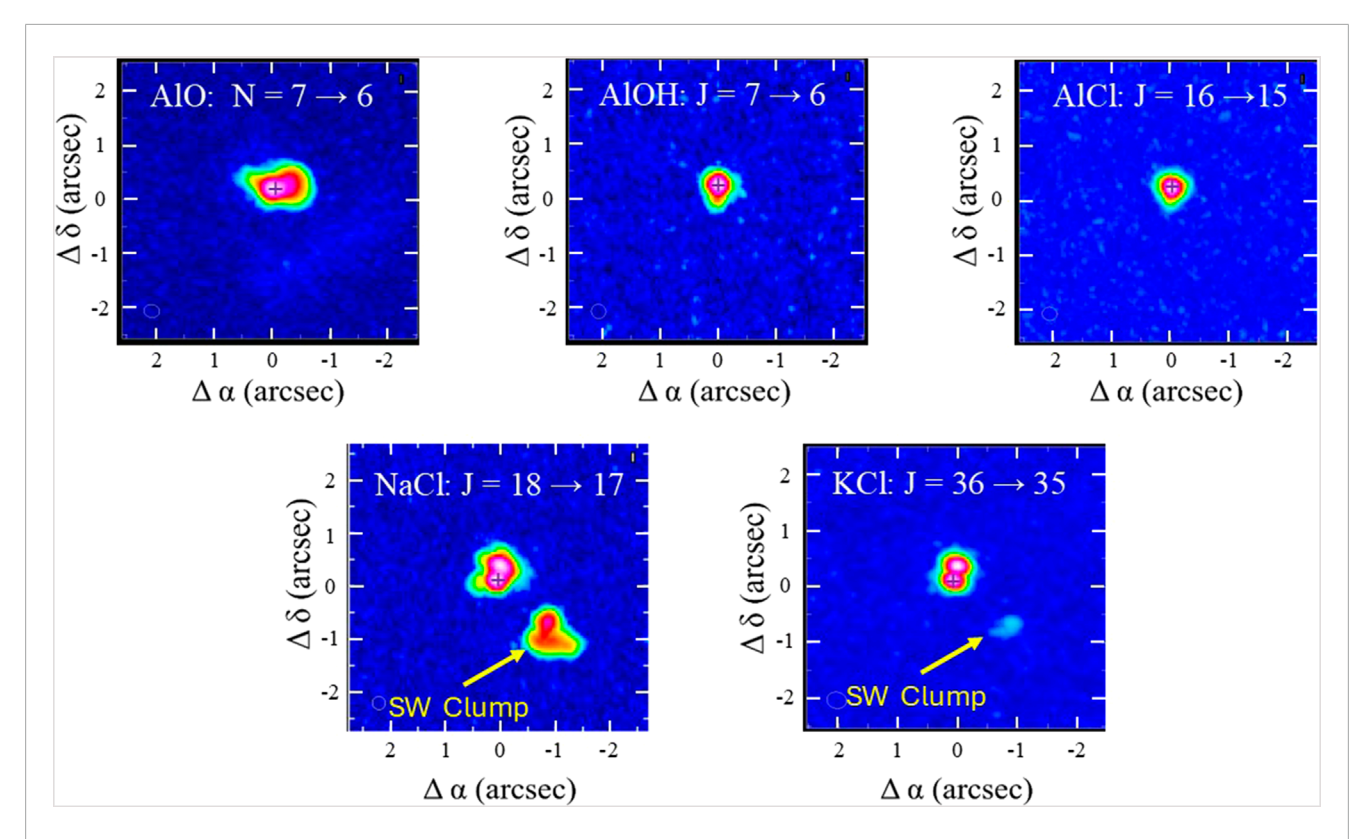


FIGURE 4 Combined ALMA/SMT images of VY CMa of (upper) AlO ($N=7\rightarrow 6$), AlOH ($J=7\rightarrow 6$), AlCl ($J=16\rightarrow 15$), (lower) NaCl ($J=18\rightarrow 17$), and KCl ($J=36\rightarrow 35$), plotted on the same spatial scale of ~2.5" \times 2.5" (Ravi et al., 2025a; Ravi et al., 2025b). Crosses indicate the stellar position. The synthesized beams are shown in the lower left-hand corners. Maximum flux (Jy/beam; in pink) is 0.12 for AlO and NaCl, 0.05 for AlOH, and 0.04 for AlCl and KCl. All five molecules are located within the LTE zone. NaCl and KC also highlight the SW Clump.

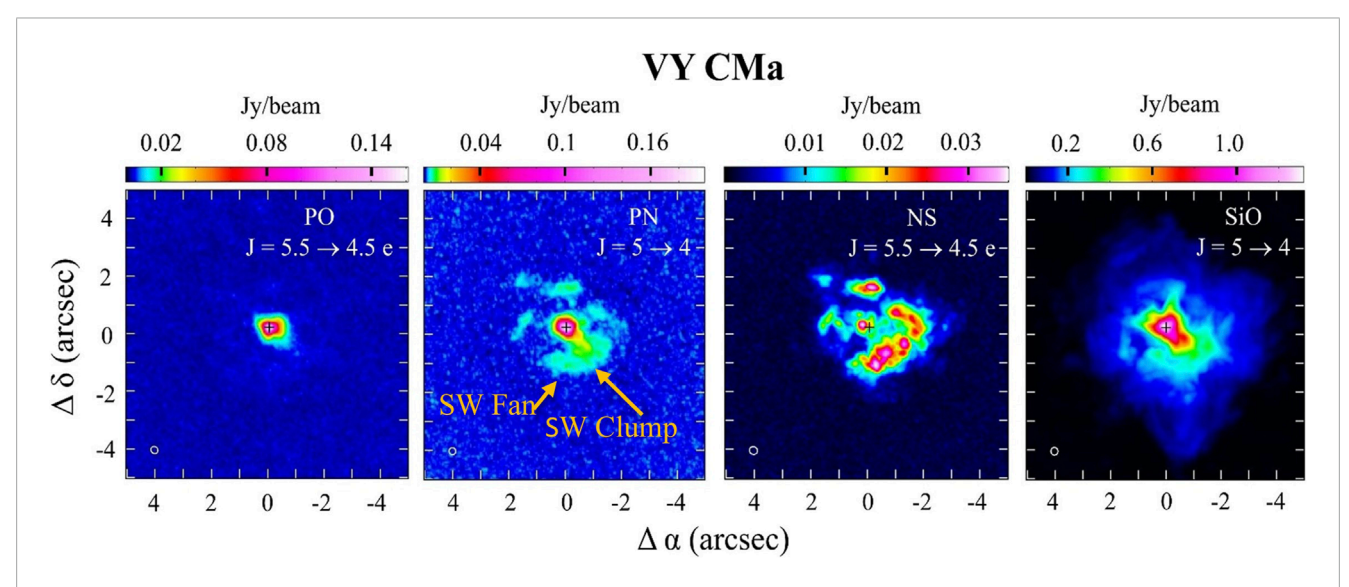


FIGURE 5 Combined ALMA/SMT images of (*left to right*) PO (J = 5.5 \rightarrow 4.5 e transition, PN (J = 5 \rightarrow 4), NS (J = 5.5 \rightarrow 4.5 e), and SiO (J = 5 \rightarrow 4), plotted on the same spatial scale of \sim 5" \times 5". Synthesized beam sizes are shown at lower left; crosses indicate the stellar position. Flux scales (Jy/beam) are indicated on the figure. The data show that PO is solely centered on the star. PN has peak emission on the star as well, but also has extended structure to the SW (SW Fan) that includes the SW Clump, as indicated, and additional clumps N, E and W of the star. The distributions of NS and PN are almost identical and similar to that of SiO (Ravi et al., 2024).

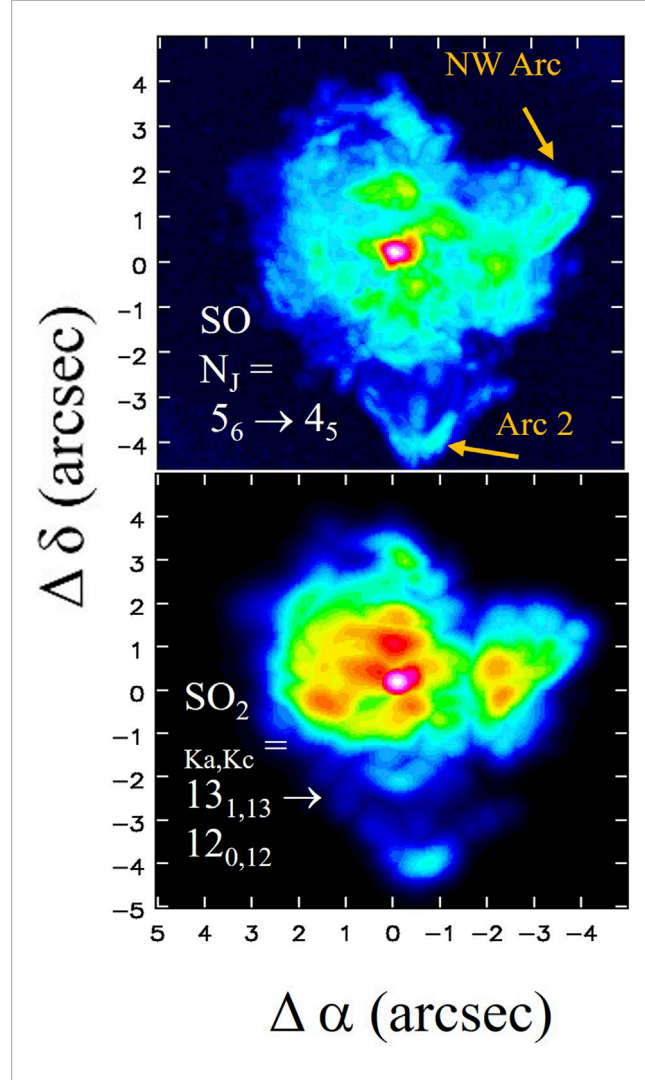


FIGURE 6 Combined ALMA/SMT images for *(upper)* SO $(N_J=5_6\rightarrow 4_5)$ and *(lower)* SO₂ $(J_{Ka,Kc}=13_{1.13}\rightarrow 12_{0.12})$, plotted on the same spatial scale of ~10" × 10." Maximum flux (Jy/beam; in pink) is 0.6 for SO and 0.5 for SO₂. While both molecules have their peak intensity centered on the star, their emission extends over 8" and clearly highlights the NW Arc and Arc 2, as indicated.

formation of the most thermodynamically stable species—usually closed-shell molecules. The synthesis of the molecules is therefore path-independent, and abundances can be estimated solely from thermodynamic data (Tsuji, 1973). These molecules typically form before the escaping gas has reached the terminal stellar velocity (Keady et al., 1988). As the gas moves from the photosphere, it cools and dust forms, which further accelerates the roughly spherical mass loss. As discussed by Cherchneff (2012), stellar pulsations can alter LTE abundances, but as a secondary effect.

The role of LTE chemistry in massive stars is well demonstrated by oxide and halide compounds in VY CMa, as shown in Figure 4. Here combined ALMA/SMT images of AlO ($N=7 \rightarrow 6$), AlOH ($J=7 \rightarrow 6$), AlCl ($J=16 \rightarrow 15$), NaCl ($J=18 \rightarrow 17$), and KCl ($J=36 \rightarrow 35$) are shown on the same spatial scale, indicated on the maps. The position of the star is shown by a cross on the AlO and NaCl images. The flux scales are given in the figure caption. All molecules have

dipole moments that are reasonably large–between 1 and 9 D - and the transitions sample the energy range 50–100 K. Hence a spatial comparison is valid. The one exception is KCl, with a dipole moment near 10 D and a high energy transition near $\sim\!250$ K.

The images of the Al-bearing molecules (top row) show that their distribution is exclusively within a radius ~0.5" or ~50-60 R* from the star. Because all flux has been recovered in the image reconstruction, this conclusion is robust. The images of AlCl and AlOH are almost identical, with a slight N-S elongation. In contrast, the distribution of AlO is somewhat larger and shows a small E-W extension. To the west, it appears to follow the direction of the NW Arc (Figure 1). The mass loss event that caused the NW Arc may have shocked and entrained the Al-molecular material coming symmetrically off the photosphere, raising the local temperature. The production of AlO is favored over that of AlCl and AlOH in LTE models only when the temperature is T ~2500 K (Tenenbaum and Ziurys, 2009), which could have occurred in the ejected and entrained material (Ravi et al., 2025a). The emission of all three aluminum molecules abruptly drops at about 50 R*, which is likely due to condensation onto dust grains. Grain formation typically begins within 10-20 R_{*}. Other species such as SO have emission well beyond this radius (Figure 6), such that conditions still support molecular excitation.

The halide species NaCl and KCl also have a confined distribution around the star, as predicted by LTE models (e.g., Milam et al., 2007; Cherchneff, 2012). Similar to the aluminum compounds, they quicky disappear from the gas phase due to grain condensation at larger distances from the star. The narrow linewidths of these two molecules indicate that they have not reached the star's terminal velocity and must disappear from the gas phase (also see Milam et al., 2007). However, the molecules both exhibit two separate peaks near the star, separated by about 0.3". These two structures show slightly red and blue-shifted velocities, respectively, with respect to the stellar velocity (~18 and 25 km s⁻¹ vs. 22 km s⁻¹). Moreover, NaCl and KCl have a secondary source approximately 1.5" SW of the star, coincident with the SW Clump feature observed in the HST dust images (Humphreys et al., 2025). This source is much weaker in KCl, but the halide has a lower abundance by about a factor of 10 (see Table 2). The secondary peak also was noted in earlier, less sensitive ALMA images of sodium chloride (Decin et al., 2016). The SW Clump source in NaCl and KCl consists also of two velocity components that link them to the S Arc and Clumps E1/E2 seen in HST KI spectra (Humphreys et al., 2025). These velocities are the same two values observed in these molecules on the stellar source, suggesting that the SW Clump structures were formed from knots ejected near the stellar photosphere and then survived reasonably intact (Ravi et al., 2025b).

Another oxide produced exclusively by LTE chemistry in VY CMa is PO, as shown in Figure 5 (far left, $J = 5.5 \rightarrow 4.5$ e transition). Note that the spatial scale has been expanded by almost a factor of two in this figure relative to Figure 4. The ALMA image shows that PO is confined to the star within ~60 R* (Ravi et al., 2024). The measured abundance of the molecule of PO/H₂ ~ 10^{-7} matches that predicted by LTE models at T ~ 1500 K–roughly the temperature at these radii (Milam et al., 2008). In contrast, the other known P-bearing species, PN, has a much more extended distribution (Figure 5, left, $J = 5 \rightarrow 4$ line). Although the bulk of its emission peaks near the star, resembling PO, a fan-like structure is also observed in

PN, extending to the SW and encompassing most of the SW Clump region. Unlike NaCl and KCl, the emission in PN is continuous from the star to the SW Clump, which in part may be a density effect (c.f., Figures 4, 5). Furthermore, PN is visible in another four distinct regions to the N, W and E of the star (Cloudlets I, II, II, IV; see Ravi et al., 2024). The complex distribution of PN is duplicated in strong emission in NS (Figure 5, right, $J = 5.5 \rightarrow 4.5$ e). NS clearly traces the "SW Fan" and the four cloudlets. As Figure 5 (far right) also shows, the $J = 5 \rightarrow 4$ line of SiO traces the SW Fan but has more extended emission beyond these regions.

PO and PN are generally produced together in energetic gas, according to most chemical models (Aota and Aikawa, 2012; Lefloch et al., 2016; Jiménez-Serra et al., 2018). They also have comparable excitation conditions with dipole moments of 1.88 D and 2.75 D, respectively. VY CMa presents an unusual situation where, in certain regions, PN is present in the absence of PO. These regions (SW Fan, Cloudlets) appear to be related to the sporadic mass loss that generated the SW Clumps and likely contain shocked gas, as indicated by the presence of SiO (Ziurys et al., 1989). As discussed in the recent models, the only instance where PN is synthesized preferentially over PO in shocked material is when there is enhanced nitrogen abundance and the timescales are short, typically a few hundred years. Apart from the models, the shocks are also needed to liberate phosphorus from the dust grains that removed the gas-phase PO and PN near the star.

The unusual coincidence of PN and NS suggests nitrogen enrichment, in agreement with the model predictions. The SW Clump material was ejected about 200 years ago (Humphreys et al., 2025), placing a similar age on the SW Fan and Cloudlets, also in line with the models. Therefore, the criteria for enhanced PN formation are fulfilled (Ravi et al., 2024). A possible route (Equation 1) to PN is from NS:

$$P + NS \rightarrow PN + S$$
 (1)

The rate for this reaction is not known. It involves two radical species, however, and it likely to be reasonably fast ($k \sim 10^{-11}~{\rm cm}^3~{\rm s}^{-1}$). Note that nitrogen enrichment can occur through dredge-up in the H-burning shell in RSGs (Levesque, 2017), which could seed individual ejecta with excess N. Evidence of this dredge-up would be enhanced $^{13}{\rm C}$, which is observed in the SW Fan (Ravi et al., 2024). Therefore, a combination of shocks, grain destruction, short ejecta timescales, and elemental enrichment from convective mixing creates the chemical environment needed for PN production in VY CMa.

The remaining question is the absence of NaCl in the SW Fan. This result in part could be due to the relative dipole moments of PN (2.75 D) vs. NaCl (9 D). NaCl might therefore be tracing only the denser material present in the SW Clump. However, the agreement in the two velocities near the star and in the SW Clump in NaCl suggests that the molecule is actually contained in the original ejected knots that formed the Clump.

Figure 6 shows ALMA images for SO $(N_J = 5_6 \rightarrow 4_5)$ and SO₂ $(J_{Ka, Kc} = 13_{1,13} \rightarrow 12_{0,12})$ on a scale of ~10". The first thing to note is that both molecules are present in a region about 8" in size, as opposed to ~4" for NS and PN. NS has a dipole moment of 1.81 D-lower than those of PN but comparable to SO (1.54 D), SO₂ (1.63 D, b-dipole), and PO. Furthermore, the upper state energies

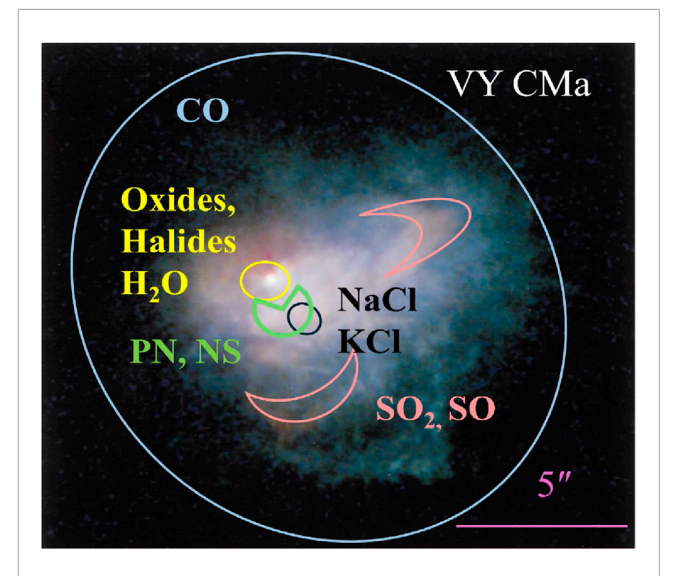


FIGURE 7
Cartoon showing the approximate locations of key molecules superimposed on the HST image. CO tracks the overall envelope structure, while oxides (AlO, AlOH, TiO, PO, SO, H₂O, SO₂) and halides (NaCl, KCl) trace the LTE zone near the star. Refractory species condense out onto dust grains at about 50 R* from the star, while the more volatile molecules disseminate in a slow moving wind. Individual mass ejecta disrupt this wind, bringing shocks, grain destruction and certain elemental enrichment to the discrete structures SW Fan and SW Clump. The older ejecta such as Arc 2 and NW Arc are lit up by SO, SO₂, and HCN (also see Singh et al., 2023).

of the transitions involved are 35 K (SO), 82 K (SO₂), 40 K (NS) and 34 K (PN). Consequently, PN and NS should be visible in gas where the observed transitions of SO and SO2 are excited. The varied distributions of these four molecules must be a consequence of chemistry. Secondly, SO and SO2 both trace HST dust structures NW Arc and Arc 2, as does CO, as well as the SW Fan and Clump regions. Because these features are created from energetic mass loss, they are likely to involve shocks of some type. The two sulfurbearing oxides in fact may be indicating the shock front in Arc 2, for example, and could be tracing swept-up material (Adande et al., 2013; Quintana-Lacaci et al., 2023). It is noteworthy that SO₂ is slightly more abundant than SO by a factor of 1.5 (see Table 2 and Adande et al., 2013). Models suggest that SO₂ can be produced in excess of SO by MHD shocks (Pineau des Forets et al., 1993). The OH radical is formed from H₂O in the shock front, and then reacts with SO to create excess SO₂ (Equation 2) in the magneticallyextended post-shock region:

$$OH + SO \rightarrow SO_2 + H$$
 (2)

Strong magnetic fields are found in VY CMa close to the star (Shinnaga et al., 2017), but their more extended presence is not known. The existence of SO and SO₂ in the dust features that are 3–5" from the star, while PN and NS have effectively disappeared, may simply be a time effect. Arc 2 and the NW Arc are older than the SW Fan, for example, and PN may have already condensed back onto grain at this juncture. The older features may also not be enriched in nitrogen, as dredge-up may be event specific.

5 An overview linking morphology and chemical processes

A qualitative diagram summarizing the chemistry in VY CMa is presented in Figure 7. Here the approximate locations of key molecules are shown against the background of the HST image. CO (and HCN: see Singh et al., 2023) trace the overall envelope structure, as shown in Figure 1. Oxides PO, AlO, AlOH, SO, SiO, H₂O, and SO₂ are found near the star (also TiO, TiO₂; see De Beck et al., 2015; Kaminski et al., 2013; Quintana-Lacaci et al., 2023), as are the halides NaCl and KCl. This region is the LTE zone. Some of the more refractory species condense out onto dust grains about 50 R* from the star (AlO, PO, AlOH), while the more volatile species such as SO and SO₂ perpetuate in a slow moving wind. Individual mass ejecta disrupt this wind, bringing shocks, grain destruction and certain elemental enrichment to discrete structures (Adande et al., 2013; Quintana-Lacaci et al., 2023). The older ejecta such as Arc 2 and NW Arc are lit up by SO, SO2, and HCN. The younger flows mark the SW Fan and the Cloudlets with enhanced nitrogen from dredge-up, highlighted by PN and NS. The SW Clump is a series of knots and bullets ejected from the star that contain NaCl and KCl, likely entrained in the material from the LTE zone.

This picture is of course simplified, and more details will emerge as other molecular images are produced and analyzed. Nonetheless, the emerging portrait of the envelope of VY CMa shows considerable complexity. It is likely that such a complicated scenario exists in other massive RSGs such as NML Cyg. Such objects need further study.

6 Conclusion

The envelopes of massive stars or RSGs, are complex chemical environments where extreme mass loss influences the molecular synthesis in a striking way. Not only do these mass loss events create shocks and disrupt the basic stellar wind, but they can cause elemental enrichment and grain destruction. They also can entrain material formed near the stellar photosphere. The Red Hypergiant stars such as VY CMa and NML Cyg appear to exhibit the highest chemical complexity, and the most energetic mass loss and highest mass loss rates (~10⁻⁴ M_o yr⁻¹). Those RSGs with lower mass rates (10⁻⁶-10⁻⁵ M_o yr⁻¹) such as Betelgeuse and VX Sgr are not nearly as chemically rich. Massive stars with high mass loss rates (~10⁻⁴ M_☉ yr⁻¹) that are moving to warmer temperatures and evolving into Yellow Hypergiants, such as IRC+10420, see a decline in molecular content, as well. YHGs appear to have a detached molecular envelope, which must influence the abundances of inner shell, LTE zone molecules. These conclusions are based on a few objects, but more studies are in progress concerning the molecular content of these remarkable envelopes, which will likely bring new insights.

Data availability statement

The datasets presented in this study can be found in online repositories. The names of the repository/repositories and accession number(s) can be found below: IOP Press.

Author contributions

LZ: Writing – original draft, Writing – review and editing.

Funding

The author(s) declare that financial support was received for the research and/or publication of this article. This research was supported by NSF Grant AST-2307305.

Acknowledgments

The author thanks R.M. Humphreys, A.M.S. Richards, R. Ravi and A.P. Singh for their collaborative efforts in understanding the envelopes of RSGs.

Conflict of interest

The author declares that the research was conducted in the absence of any commercial or financial relationships that could be construed as a potential conflict of interest.

Generative Al statement

The author(s) declare that no Generative AI was used in the creation of this manuscript.

Any alternative text (alt text) provided alongside figures in this article has been generated by Frontiers with the support of artificial intelligence and reasonable efforts have been made to ensure accuracy, including review by the authors wherever possible. If you identify any issues, please contact us.

Publisher's note

All claims expressed in this article are solely those of the authors and do not necessarily represent those of their affiliated organizations, or those of the publisher, the editors and the reviewers. Any product that may be evaluated in this article, or claim that may be made by its manufacturer, is not guaranteed or endorsed by the publisher.

References

Adande, G. R., Edwards, J. L., and Ziurys, L. M. (2013). Sulfur chemistry in the envelope of VY canis majoris: detailed analysis of SO and ${\rm SO}_2$ emission. *Astrophysical J.* 778, 22. doi:10.1088/0004-637x/778/1/22

Agúndez, M., Cernicharo, J., Quintana Lacaci, G., Castro-Carrizo, A., Velilla Prieto, L., Marcelino, N., et al. (2017). Growth of carbon chains in IRC +10216 mapped with ALMA. *Astronomy Astrophysics* 601, A4. doi:10.1051/0004-6361/201630274

Andrews, H., De Beck, E., and Hirvonen, P. (2022). Multiple components in the molecular outflow of the red supergiant NML Cyg. *Mon. Notices R. Astronomical Soc.* 510, 383–398. doi:10.1093/mnras/stab3244

Aota, T., and Aikawa, Y. (2012). Phosphorus chemistry in the shocked region L1157 B1. Astrophysical J. 761, 74. doi:10.1088/0004-637x/761/1/74

Asplund, M., Grevesse, N., Sauval, A. J., and Scott, P. (2009). The chemical composition of the sun. *Annu. Rev. Astronomy Astrophysics* 47, 481–522. doi:10.1146/annurev.astro.46.060407.145222

Bachiller, R., Fuente, A., Bujarrabal, V., Colomer, F., Loup, C., et al. (1997). A survey of CN in circumstellar envelopes. *Astronomy Astrophysics* 319, 235–243.

Baudry, A., Wong, K. T., Etoka, S., Richards, A. M. S., Mueller, H. S. P., Herpin, F., et al. (2023). ATOMIUM: probing the inner wind of evolved O-rich stars with new, highly excited H2O and OH lines. *Astronomy and Astrophysics* 674, A125. doi:10.1051/0004-6361/202245193

Cernicharo, J., and Guelin, M. (1987). Metals in IRC \pm 10216: detection of NaCl, AlCl, and KCl, and tentative detection of AlF. Astronomy Astrophysics 183, L10–L12.

Cherchneff, I. (2012). The inner wind of IRC+10216 revisited: new exotic chemistry and diagnostic for dust condensation in carbon stars. Astronomy Astrophysics 545, A12. doi:10.1051/0004-6361/201118542

De Beck, E., Vlemmings, W., Muller, S., Black, J. H., O'Gorman, E., Richards, A. M. S., et al. (2015). ALMA observations of ${\rm TiO_2}$ around VY Canis majoris. *Astronomy Astrophysics*. 580, A36. doi:10.1051/0004-6361/201525990

De Beck, E., Andrews, H., Quintana-Lacaci, G., and Vlemmings, W. H. T. (2025). The circumstellar environment around the extreme galactic red supergiant NML Cygni: dense, dusty, and asymmetric. *Astronomy and Astrophysics* 698, A179. doi:10.1051/0004-6361/202554748

Decin, L., Hony, S., de Koter, A., Justtanont, K., Tielens, A. G. G. M., and Waters, L. B. F. M. (2006). Probing the mass-loss history of AGB and red supergiant stars from CO rotational line profiles. I. Theoretical model - mass-loss history unravelled in VY CMa. Astronomy Astrophysics 456, 549–563. doi:10.1051/0004-6361: 20065230

Decin, L., Richards, A. M. S., Millar, T. J., Baudry, A., De Beck, E., Homan, W., et al. (2016). ALMA-resolved salt emission traces the chemical footprint and inner wind morphology of VY Canis Majoris. *Astronomy and Astrophysics* 592, A76. doi:10.1051/0004-6361/201527934

Ekstrom, S., and Georgy, C. (2025). Stellar evolution through the red supergiant phase. Galaxies.~13, 81.~doi:10.3390/galaxies13040081

Goldsmith, P. F., Irvine, W. M., Hjalmarson, A., and Ellder, J. (1986). Variations in the HCN/HNC abundance ratio in the orion molecular cloud. *Astrophysical J.* 310, 383–391. doi:10.1086/164692

Gordon, M. S., and Humphreys, R. M. (2019). Red supergiants, yellow hypergiants, and Post-RSG evolution. Galaxies~7,92.~doi:10.3390/galaxies7040092

Herwig, F. (2005). Evolution of asymptotic giant branch stars. *Annu. Rev. Astronomy Astrophysics* 43, 435–479. doi:10.1146/annurev.astro.43.072103.150600

Höfner, S., and Olofsson, H. (2018). Mass loss of stars on the asymptotic giant branch. Mechanisms, models and measurements. *Astronomy Astrophysics Rev.* 26, 1. doi:10.1007/s00159-017-0106-5

Humphreys, R. M., and Jones, T. J. (2022). Episodic gaseous outflows and mass loss from red supergiants. *Astronomical J.* 163, 103. doi:10.3847/1538-3881/ac46ff

Humphreys, R. M., Helton, L. A., and Jones, T. J. (2007). The three-dimensional morphology of VY Canis Majoris. I. The kinematics of the ejecta. *Astronomical J.* 133, 2716–2729. doi:10.1086/517609

Humphreys, R. M., Ziurys, L. M., Bernal, J. J., Gordon, M. S., Helton, L. A., Ishibashi, K., et al. (2019). The unexpected spectrum of the innermost ejecta of the red hypergiant VY CMa. *Astrophysical J. Lett.* 874, L26. doi:10.3847/2041-8213/ab11e5

Humphreys, R. M., Jones, T. J., Davidson, K., Richards, A. M. S., Ravi, R., Singh, A. P., et al. (2025). The Infrared-bright SW knots in the complex ejecta of VY CMa. *Astronomical J.* 169, 230. doi:10.3847/1538-3881/adbbf1

Jiménez-Serra, I., Viti, S., Quénard, D., and Holdship, J. (2018). The chemistry of phosphorus-bearing molecules under energetic phenomena. *Astrophysical J.* 862, 128. doi:10.3847/1538-4357/aacdf2

Kaminski, T., Gottlieb, C. A., Menten, K. M., Patel, N. A., Young, K. H., Brünken, S., et al. (2013). Pure rotational spectra of TiO and ${\rm TiO_2}$ in VY Canis majoris. *Astronomy and Astrophysics* 551, A113. doi:10.1051/0004-6361/201220290

Keady, J. J., Hall, D. N. B., and Ridgway, S. T. (1988). The IRC +10216 circumstellar envelope. I. Models for the dust and gas. *Astrophysical J.* 326, 832–842. doi:10.1086/166141

Kwok, S. (2016). Physics and chemistry of the late stages of stellar evolution — an introduction. $\it JPhCS$ 728, 022001. doi:10.1088/1742-6596/728/2/022001

Lefloch, B., Vastel, C., Viti, S., Jimenez-Serra, I., Codella, C., Podio, L., et al. (2016). Phosphorus-bearing molecules in solar-type star-forming regions: first PO detection. *Mon. Notices R. Astronomical Soc.* 462, 3937–3944. doi:10.1093/mnras/stw1918

Levesque, E. M. (2017). Astrophysics of red supergiants. IOP Publishing.

Lim, J., Carilli, C. L., White, S. M., Beasley, A. J., and Marson, R. G. (1998). Large convection cells as the source of Betelgeuse's extended atmosphere. *Nature* 392, 575–577. doi:10.1038/33352

McCabe, E. M., Smith, R. C., and Clegg, R. E. S. (1979). Molecular abundances in IRC + 10216. Nature 281, 263–266. doi:10.1038/281263a0

Menten, K. M., Wyrowski, F., Alcolea, J., De Beck, E., Decin, L., Marston, A. P., et al. (2010). Herschel/HIFI deepens the circumstellar NH₃ enigma. *Astronomy Astrophysics* 521, L7. doi:10.1051/0004-6361/201015108

Milam, S. N., Apponi, A. J., Woolf, N. J., and Ziurys, L. M. (2007). Oxygen-rich mass loss with a pinch of salt: NaCl in the circumstellar gas of IK Tauri and VY Canis Majoris. *Astrophysical J.* 668, L131–L134. doi:10.1086/522928

Milam, S. N., Halfen, D. T., Tenenbaum, E. D., Apponi, A. J., Woolf, N. J., and Ziurys, L. M. (2008). Constraining phosphorus chemistry in Carbon- and oxygen-rich circumstellar envelopes: observations of PN, HCP, and CP. Astrophysical J. 684, 618–625. doi:10.1086/589135

Milam, S. N., Woolf, N. J., and Ziurys, L. M. (2009). Circumstellar $^{12}C/^{13}C$ isotope ratios from millimeter observations of CN and CO: mixing in carbon- and oxygen-rich stars. *Astrophysical J.* 690, 837–849. doi:10.1088/0004-637x/690/1/837

Neufeld, D. A., Menten, K. M., Duran, C., Guesten, R., Kaufman, M. J., Kraus, A., et al. (2021). Terahertz water masers. II. Further SOFIA/GREAT detections toward circumstellar outflows, and a multitransition analysis. *Astrophysical J.* 907, 42. doi:10.3847/1538-4357/abc628

Omont, A., Lucas, R., Morris, M., and Guilloteau, S. (1993). S-bearing molecules in O-rich circumstellar envelopes. *Astronomy Astrophysics* 267, 490–514.

Pineau des Forets, G., Roueff, E., Schilke, P., and Flower, D. R. (1993). Sulphur-bearing molecules as tracers of shocks in interstellar clouds. *Mon. Notices R. Astronomical Soc.* 262, 915–928. doi:10.1093/mnras/262.4.915

Quintana-Lacaci, G., Bujarrabal, V., Castro-Carrizo, A., and Alcolea, J. (2007). The chemical composition of the circumstellar envelopes around yellow hypergiant stars. *Astronomy Astrophysics* 471, 551–560. doi:10.1051/0004-6361:20077244

Quintana-Lacaci, G., Agundez, M., Cernicharo, J., Bujarrabal, V., Sanchez Contreras, C., Castro-Carrizo, A., et al. (2016). A 3 mm and 1 mm line survey toward the yellow hypergiant IRC +10420. N-rich chemistry and IR flux variations. *Astronomy and Astrophysics* 592, A51. doi:10.1051/0004-6361/201527688

Quintana-Lacaci, G., Velilla Prieto, L., Agúndez, M., Fonfría, J. P., Cernicharo, J., Agúndez, M., et al. (2023). History of two mass loss processes in VY CMa. *Astronomy Astrophysics* 669, A56. doi:10.1051/0004-6361/202244396

Ravi, R., Singh, A. P., Richards, A. M. S., Humphreys, R. M., Decin, L., and Ziurys, L. M. (2024). PO and PN in the envelope of VY Canis Majoris: elucidating the chemistry and origin of phosphorus. *Astrophysical J. Lett.* 971, L43. doi:10.3847/2041-8213/ad6660

Ravi, R., Richards, A. M. S., Humphreys, R. M., and Ziurys, L. M. (2025a). Aluminum chemistry in the envelope of VY Canis Majoris: an ALMA perspective. *Astrophysical J.* Submitted.

Ravi, R., Richards, A. M. S., Humphreys, R. M., and Ziurys, L. M. (2025b). Salt chemistry in the outflows of VY Canis Majoris. $Astrophysical\ J$. Submitted.

Royer, P., Decin, L., Wesson, R., Barlow, M. J., Polehampton, E. T., Matsuura, M., et al. (2010). PACS and SPIRE spectroscopy of the red supergiant VY CMa. *Astronomy Astrophysics* 518, L145. doi:10.1051/0004-6361/201014641

Sanchez Contreras, C., Velilla Prieto, L., Cernicharo, J., Agúndez, M., Quintana-Lacaci, G., et al. (2015). Molecular ions in the O-rich evolved star OH231.8+4.2: HCO^+ , $H^{13}CO^+$ and first detection of SO^+ , N_2H^+ , and H_3O^+ . Astronomy Astrophysics 577, A52. doi:10.1051/0004-6361/201525652

Shinnaga, H., Claussen, M. J., Yamamoto, S., and Shimojo, M. (2017). Strong magnetic field generated by the extreme oxygen-rich red supergiant VY Canis Majoris. *Publ. Astronomical Soc. Jpn.* 69, L10. doi:10.1093/pasj/psx110

Singh, A. P., Edwards, J. L., Humphreys, R. M., and Ziurys, L. M. (2021). Molecules and outflows in NML Cygni: new insights from a 1 mm spectral line survey. Astrophysical J. Lett. 920, L38. doi:10.3847/2041-8213/ac2c7c

Singh, A. P., Edwards, J. L., and Ziurys, L. M. (2022). The Arizona radio observatory 1 mm spectral survey of the hypergiant star NML Cygni (215-285 GHz). *Astronomical J.* 164, 230. doi:10.3847/1538-3881/ac8df0

Singh, A. P., Richards, A. M. S., Humphreys, R. M., Decin, L., and Ziurys, L. M. (2023). ALMA reveals hidden morphologies in the molecular envelope of VY Canis Majoris. *Astrophysical J. Lett.* 954, L1. doi:10.3847/2041-8213/ace7cb

Smartt, S. J. (2015). Observational constraints on the progenitors of core-collapse supernovae: the case for missing high-mass stars. *Publ. Astronomical Soc. Aust.* 32, e016. doi:10.1017/pasa.2015.17

Smith, N. A. (2014). Mass loss: its effect on the evolution and fate of high-mass stars. Annu. Rev. Astronomy Astrophysics 52, 487–528. doi:10.1146/annurev-astro-081913-040025

Tenenbaum, E. D., and Ziurys, L. M. (2009). Millimeter detection of AlO ($X^2\Sigma^+$): metal oxide chemistry in the envelope of VY Canis majoris. *Astrophysical J. Lett.* 694, L59–L63. doi:10.1088/0004-637x/694/1/159

Tenenbaum, E. D., and Ziurys, L. M. (2010). Exotic metal molecules in oxygen-rich envelopes: detection of AlOH ($X^1\Sigma^+$) in VY Canis majoris. Astrophysical J. Lett. 712, L93–L97. doi:10.1088/2041-8205/712/1/l93

Tenenbaum, E. D., Woolf, N. J., and Ziurys, L. M. (2007). Identification of phosphorus monoxide ($X^2\Pi r$) in VY canis majoris: detection of the first PO bond in space. Astrophysical J. Lett. 666, L29–L32. doi:10.1086/521361

Tenenbaum, E. D., Dodd, J. L., Milam, S. N., Woolf, N. J., and Ziurys, L. M. (2010a). Comparative spectra of oxygen-rich versus carbon-rich circumstellar shells: VY Canis majoris and IRC+ 10216 at 215–285 GHz. Astrophysical J. Lett. 720, L102–L107. doi:10.1088/2041-8205/720/1/102

Tenenbaum, E. D., Dodd, J. L., Milam, S. N., Woolf, N. J., and Ziurys, L. M. (2010b). The Arizona radio observatory 1 mm spectral survey of IRC+ 10216 and VY Canis majoris (215–285 GHz). *Astrophysical J. Suppl. Ser.* 190, 348–417. doi:10.1088/0067-0049/190/2/348

Teyssier, D., Quintana-Lacaci, G., Marston, A. P., Bujarrabal, V., Alcolea, J., Cernicharo, J., et al. (2012). Herschel/HIFI observations of red supergiants and yellow hypergiants. I. Molecular inventory. *Astronomy and Astrophysics* 545, A99. doi:10.1051/0004-6361/201219545

Tsuji, T. (1973). Molecular abundances in stellar atmospheres. II. Astronomy Astrophysics 23, 411–431.

Velilla Prieto, L., Sanchez Contreras, C., Cernicharo, J., Agundez, M., Quintana-Lacaci, G., Bujarrabal, V., et al. (2017). The millimeter IRAM-30 m line survey toward IK tauri. *Astronomy and Astrophysics* 597, A25. doi:10.1051/0004-6361/201628776

Verheyen, L., Messineo, M., and Menten, K. M. (2012). SiO maser emission from red supergiants across the galaxy. I. Targets in massive star clusters. *Astronomy and Astrophysics* 541, A36. doi:10.1051/0004-6361/201118265

Wallström, S. H. J., Danilovich, T., Mueller, H. S. P., Gottlieb, C. A., Maes, S., Van de Sande, M., et al. (2024). ATOMIUM: molecular inventory of 17 oxygen-rich evolved stars observed with ALMA. Astronomy Astrophysics 681, A50. doi:10.1051/0004-6361/202347632

Willacy, K., and Cherchneff, I. (1998). Silicon and sulphur chemistry in the inner wind of IRC+10216. Astronomy Astrophysics 330, 676–684.

Zhang, X., Zhu, Q., Li, J., Chen, X., Wang, J., and Zhang, J. S. (2017). A spectral line survey of IRC +10216 between 13.3 and 18.5 GHz. Astronomy and Astrophysics 606, A74. doi:10.1051/0004-6361/201730791

Ziurys, L. M. (1987). Detection of interstellar PN: the first Phosphorus-bearing species observed in molecular clouds. *Astrophysical J. Lett.* 321, L81–L84. doi:10.1086/185010

Ziurys, L. M. (2006). The chemistry in circumstellar envelopes of evolved stars: following the origin of the elements to the origin of life. *Proc. Natl. Acad. Sci.* 103, 12274–12279. doi:10.1073/pnas.0602277103

Ziurys, L. M. (2024). Prebiotic astrochemistry from astronomical observations and laboratory spectroscopy. *Annu. Rev. Phys. Chem.* 75, 307–327. doi:10.1146/annurev-physchem-090722-010849

Ziurys, L. M., and Richards, A. M. S. (2025). Molecules and chemistry in red supergiants. *Galaxies* 13, 82. doi:10.3390/galaxies13040082

Ziurys, L. M., Friberg, P., and Irvine, W. M. (1989). Interstellar SiO as a tracer of high-temperature chemistry. *Astrophysical J.* 343, 201–207. doi:10.1086/167696

Ziurys, L. M., Milam, S. N., Apponi, A. J., and Woolf, N. J. (2007). Chemical complexity in the winds of the oxygen-rich supergiant star VY Canis majoris. *Nature* 447, 1094–1097. doi:10.1038/nature05905

Ziurys, L. M., Tenenbaum, E. D., Pulliam, R. L., Woolf, N. J., and Milam, S. N. (2009). Carbon chemistry in the envelope of VY canis Majoris: implications for oxygen-rich evolved stars. *Astrophysical J.* 695, 1604–1613. doi:10.1088/0004-637x/695/2/1604

Ziurys, L. M., Schmidt, D. R., and Bernal, J. J. (2018). New circumstellar sources of PO and PN: the increasing role of phosphorus chemistry in Oxygen-rich stars. *Astrophysical J.* 856, 169. doi:10.3847/1538-4357/aaafc6